Smectogenic Copper(II) Complexes of *N*-Salicylideneaniline Derivatives. A Comparative Study of Homologous Series Carrying Alkoxy and/or Alkanoyloxy Substituents

Naomi Hoshino,*,† Kenta Takahashi,† Toshinobu Sekiuchi,† Hiromi Tanaka,† and Yoshio Matsunaga‡

Department of Chemistry, Faculty of Science, Hokkaido University, Sapporo 060, Japan, and Department of Materials Science, Kanagawa University, Tsuchiya, Hiratsuka, Kanagawa 259-12, Japan

Received August 20, 1997

A series of bis[4-alkoxy-*N*-(4-ethoxyphenyl)salicylaldiminato]copper(II) complexes have been prepared and shown to possess smectic A phases with isotropization temperatures ranging from 157 to 182 °C over butoxy to octadecyloxy homologues. Corresponding series of the ligands have also been isolated and characterized for their mostly nematogenic properties. Analogous series of bis[4-alkoxy-*N*-(4-acetoxyphenyl)salicylaldiminato]-copper(II) complexes and their ligands have also proved to be mesomorphic; both of the phase type and the thermal stability are similar to those of the *N*-(4-ethoxyphenyl) counterparts. On the other hand, a series of bis[4-alkanoyloxy-*N*-(4-ethoxyphenyl)salicylaldiminato]copper(II) complexes, in which terminal alkyl groups are attached to the 4-oxysalicylidene groups via carbonyl groups, have been shown to melt at high temperatures (184−228 °C) and not mesogenic at all, while the phase behavior of the ligand series is very similar to that of the above 4-alkoxy series. An X-ray powder diffraction study of the two series of metallosmectic phases has led to a common structural model, in which layers of bis[*N*-phenylsalicylaldiminato]copper(II) cores are intervened by fully interdigitated alkyl chains. The thermodynamic parameters for the first series have been analyzed for their dependence on the terminal alkyl chain length and partial ordering of short chains is suggested.

Introduction

The mesomorphic properties of transition metal complexes have not yet been fully exploited, while the great potential of metallomesogens as advanced molecular materials has been pointed out.[1] The kind of metal atoms and the type of ligands in reported examples have become quite diverse over the past decade.[2] What is presently needed are more systematic studies in order to establish structure−function relationships and molecular design principles toward specific material functions. In our efforts concerning mesogens of the type bis[4-X-*N*-(4-Y-phenyl)salicylaldiminato]copper(II), we described the liquid crystalline property of the complexes with X = 4-alkoxybenzoyloxy and Y = ethoxy (three-ring ligand type) exhibiting nematic and/or smectic C phases.[3] When the whole *N*-(4-Y-phenyl) moiety was replaced by the *N*-*n*-propyl group, the smectic phase was totally suppressed in the resulting complexes of *N*-alkyl two-ring ligands.[4] A modification into another two-ring ligand type is possible by removing benzoyloxy moiety from group X. Complexes of such *N*-phenyl derivatives are the subject of this paper.

The design of the complex with X = Y = alkoxy was first tested for its mesogenicity by Ovchinnikov et al. and shown to be smectogenic.[5] Other workers have since employed either four long alkoxy chains[6] or two alkoxy (= X) and two alkyl (= Y) chains.[7] Our interest is in the effect on the mesomorphism of making the rigid core structure less anisotropic (compared to our previous cases) while maintaining the elongated overall molecular shape. Therefore, a series was chosen so that group X is longer than group Y throughout ($n > 2$ in **Cu1**-*n* and **L1**-*n*; Figure 1).

Another point of our interest is in the mode of alkyl group linkage to the rigid core. Esterification reaction using aliphatic acids is a favorable procedure in liquid crystal synthesis, and the polar nature of the carbonyl group plays a vital role in ferroelectric liquid crystals (FLC). However, this polarity can affect the mesomorphic and physicochemical properties of metal complexes in an unpredictable manner. Metal−salicylaldimine FLCs are already available,[8] but it is not certain whether their

† Hokkaido University.
‡ Kanagawa University.

(1) (a) Giroud-Godquin, A.-M.; Maitlis, P. M. *Angew. Chem., Int. Ed. Engl.* **1991**, *30*, 375. (b) Bruce, D. W. *J. Chem. Soc., Dalton Trans.* **1993**, 2983.
(2) (a) Espinet, P.; Esteruelas, M. A.; Oro, L. A.; Serrano, J. L.; Sola, E. *Coord. Chem. Rev.* **1992**, *117*, 215. (b) Bruce, D. W. In *Inorganic Materials*; Bruce, D. W., O'Hare, D., Eds.; Wiley: Chichester, U.K., 1992. (c) Hudson, S. A.; Maitlis, P. M. *Chem. Rev.* **1993**, *93*, 861. (d) Polishchuk, A. P.; Timofeeva, T. V. *Russ. Chem. Rev.* **1993**, *62*, 291. (e) *Metallomesogens: Synthesis, Properties, and Applications*; Serrano, J. L., Ed.; VCH: Weinheim, 1996.
(3) Hoshino, N.; Murakami, H.; Matsunaga, Y., Inabe, T.; Maruyama, Y. *Inorg. Chem.* **1990**, *29*, 1177.
(4) Hoshino, N.; Hayakawa, R.; Shibuya, T.; Matsunaga, Y. *Inorg Chem.* **1990**, *29*, 5129.
(5) Ovchinnikov, I. V.; Galyametdinov, Y. G.; Ivanova, G. I.; Yagforava, L. M. *Dokl. Akad. Nauk SSSR* **1984**, *276*, 126.
(6) (a) Carfagna, C.; Caruso, U.; Roviello, A.; Sirigu, A. *Macromol. Chem. Rapid Commun.* **1987**, *8*, 345. (b) Caruso, U.; Roviello, A.; Sirigu, A. *Liq. Cryst.* **1988**, *3*, 1515. (c) Marcos, M.; Romero, P.; Serrano, J. L.; Bueno, V.; Cabeza, J. A.; Oro, L. A. *Mol. Cryst. Liq. Cryst.* **1989**, *167*, 123. (d) Alonso, P. J.; Marcos, M.; Martinez, J. I.; Orera, V. M.; Sanjuan, M. L.; Serrano, J. L. *Liq. Cryst.* **1993**, *13*, 585.
(7) (a) Ghedini, M.; Armentano, S.; Bartolino, R.; Rustichelli, F.; Torquati, G.; Kirov, N.; Petrov, M. *Mol. Cryst. Liq. Cryst.* **1987**, *151*, 75. (b) Ghedini, M.; Armentano, S.; Bartolino, R.; Kirov, N.; Petrov, M.; Nenova, S. *J. Mol. Liq.* **1988**, *38*, 207. (c) Torquati, G.; Francescangeli, O.; Ghedini, M.; Armentano, S.; Nicolletta, F. P.; Bartolino, R. *Nuovo Cimento* **1990**, *12*, 1363. (d) Ghedini, M.; Morrone, S.; Gatteschi, D.; Zanchini, C. *Chem. Mater.* **1991**, *3*, 752.

S0020-1669(97)01056-2 CCC: $15.00
Published on Web 03/09/1998

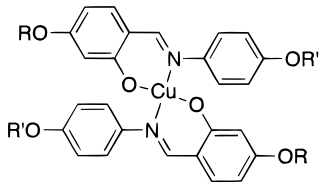

Cu-*n* (*n* = 3—12, 14, 16, 18)

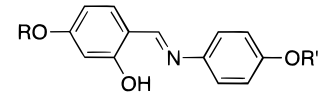

L-*n* (*n* = 3—12, 14, 16, 18)

Cu1-*n*, **L1**-*n* R = $H(CH_2)_n$-, R'= $-C_2H_5$
Cu2-*n*, **L2**-*n* R = $H(CH_2)_n$-, R'= $-COCH_3$
Cu3-*n*, **L3**-*n* R = $H(CH_2)_{n-1}CO$-, R'= $-C_2H_5$

Figure 1. Structures of the compounds studied.

dipolar ordering mechanisms are unique to metal complexes. To assess the effects of having polarized bonds in the salicylaldimine chelates, we have conducted a comparative study by preparing analogous series, as shown in Figure 1, in which either set of alkyl groups, R or R′, in **Cu1**-*n* and **L1**-*n* were replaced by alkanoyl groups (R′ = acetyl for **Cu2**-*n* and **L2**-*n* and R = alkanoyl for **Cu3**-*n* and **L3**-*n*).

Results and Discussion

Mesomorphism. Three series each of the ligands and of the copper complexes were synthesized by conventional procedures and subjected to hot-stage microscopic observation. All of the ligands, **L1**-*n*, **L2**-*n*, and **L3**-*n*, but only two series of complexes, **Cu1**-*n* (*n* = 4−18) and **Cu2**-*n* (*n* = 6−18), turned out to be mesomorphic. Table 1 summarizes the phase transition temperatures and enthalpies determined by the differential scanning calorimetry (DSC, scanning rate = ±5 K min^{-1}). Phase symbols of K, SmC, SmA, N, and I are used to denote crystalline, smectic C, smectic A, nematic, and isotropic liquid phases, respectively. Crystalline polymorphism was often observed for solution-crystallized samples, and a form of the highest melting temperature observed is numbered as in K_1 (see Experimental Procedures). The square brackets indicate a monotropic transition. Phase identification was based on the optical textures, and the magnitude of the isotropization enthalpies is consistent with the assignment of each mesophase type. Figures 2−7 show "phase pattern diagrams" which graphically compare the phase behaviors of homologous series. Alkyl tail elongation works as a weak perturbation on the intermolecular forces necessary for the mesophase formation, and the phase pattern diagram would represent the mesogenicity of a given molecular framework without complications due to an accidental anomaly in homologues of one's choice.

The series **Cu1** and **Cu2** are purely smectogenic (Figures 2 and 3). Homeotropic alignment of the molecules on a clean glass plate was commonly observed, and fan-shaped textures could be observed in some cases on cooling the isotropic liquid. This suggests strongly that the phase is of orthogonal smectic type, and X-ray diffraction profiles were consistent for all of the homologues (vide infra). The clearing temperatures are generally higher for series **Cu2** than for **Cu1**, as well as for the melting temperatures of lower homologous members.

On the other hand, the ligand series **L1** is mostly nematogenic (Figure 5), as evidenced by the marble and/or Schlieren textures. Only the two highest homologues **L1**-*n* (*n* = 16, 18) exhibit SmA phases. It is noted upon inspection of Figure 6 that the smectic behavior is enhanced in series **L2**; a new SmC phase area, detected in **L2**-*n* (*n* = 9−18), is about to emerge. The

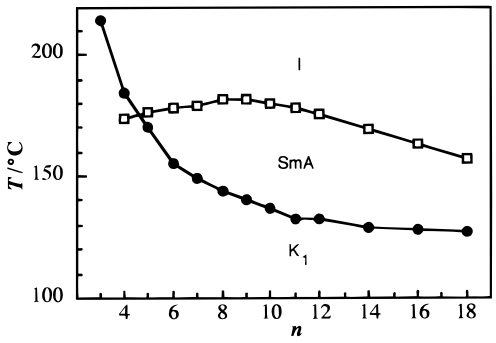

Figure 2. Phase pattern diagram for the homologous series **Cu1**.

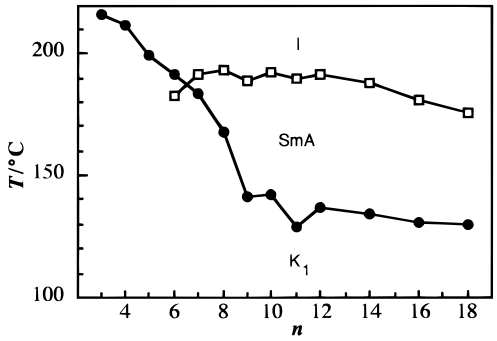

Figure 3. Phase pattern diagram for the homologous series **Cu2**.

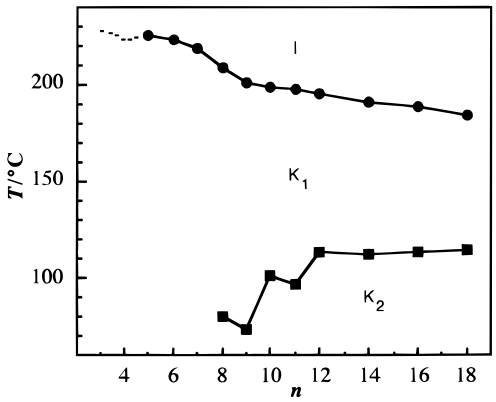

Figure 4. Phase pattern diagram for the homologous series **Cu3**.

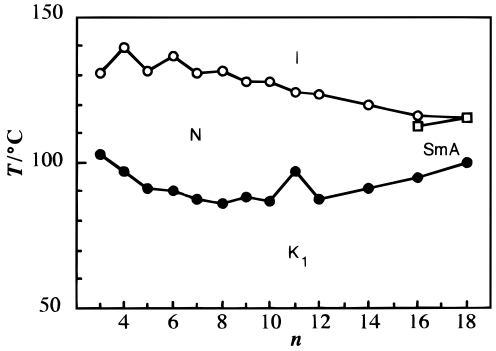

Figure 5. Phase pattern diagram for the homologous series **L1**.

(8) (a) Marcos, M.; Serrano, J. L.; Sierra, T.; Gimenez, M. J. *Angew. Chem., Int. Ed. Engl.* **1992**, *31*, 1471. (b) Marcos, M.; Serrano, J. L.; Sierra, T.; Gimenez, M. J. *Chem. Mater.* **1993**, *5*, 1332. (c) Iglesias, R.; Marcos, M.; Serrano, J. L.; Sierra, T.; Perez-Jubindo, M. A. *Chem. Mater.* **1996**, *8*, 2611.

Table 1. Mesomorphic Phase Transition Temperatures (T) and Enthalpies (ΔH) for the Compounds Prepared in This Work

compds	T/°C (ΔH/kJ mol^{-1})								compds	T/°C (ΔH/kJ mol^{-1})												
n	K_2		K_1		SmC	SmA		N	I	*n*	K_2		K_1		SmC		SmA			N		I
Cu1-*n*										**L1**-*n*												
3			·	214.1 (62)[a]					·	3			·	103.1 (31)						·	130.7 (0.96)	·
4			·	184.8 (61)[a]		[·	174.3 (*b*)]		·	4			·	96.7 (30)						·	139.8 (1.4)	·
5			·	170.0 (51)		·	176.1 (8.6)		·	5			·	90.7 (32)						·	131.2 (0.97)	·
6	·	126 (2.7)	·	155.6 (48)		·	178.1 (9.2)		·	6			·	90.4 (31)						·	136.6 (1.6)	·
7			·	148.8 (48)		·	179.4 (9.8)		·	7	·	54 (8.3)	·	87.2 (33)						·	130.7 (1.2)	·
8	·	125 (2.7)	·	143.7 (46)		·	181.9 (10)		·	8	·	47 (7.9)	·	86.2 (33)						·	131.1 (1.7)	·
9	·	123 (3.1)	·	140.5 (46)		·	181.6 (11)		·	9			·	88.1 (50)						·	127.9 (1.3)	·
10			·	136.7 (53)		·	180.4 (11)		·	10	·	76 (12)	·	86.4 (35)						·	127.9 (2.0)	·
11			·	132.3 (55)		·	178.1 (11)		·	11			·	97.0 (60)						·	123.9 (1.6)	·
12			·	132.3 (58)		·	175.8 (11)		·	12			·	87.6 (54)						·	123.4 (2.2)	·
14	·	54 (6.6)	·	129.2 (66)		·	169.5 (11)		·	14			·	91.4 (62)						·	119.6 (2.9)	·
16	·	67 (9.9)	·	127.9 (74)		·	163.4 (11)		·	16			·	94.8 (70)			·	112.6 (*h*)		·	116.3 (4.0)	·
18	·	76 (*c*)	·	127.0 (76)		·	157.3 (11)		·	18			·	99.6 (77)			·	115.4 (4.4)				·
Cu2-*n*										**L2**-*n*												
3	·	139 (5.6)	·	215.9 (50)[a]					·	3			·	104.6 (22)						·	114.7 (0.79)	·
4	·	169 (9.4)	·	211.7 (40)[a]					·	4			·	99.7 (33)						·	125.7 (1.2)	·
5			·	199.8 (38)[a]					·	5			·	110.7 (47)						·	116.8 (0.82)	·
6			·	191.2 (40)		[·	183.1 (5.1)[a]]		·	6			·	83.8 (30)						·	120.2 (1.3)	·
7			·	183.6 (36)		·	191.7 (*d*)		·	7			·	87.1 (26)						·	116.1 (1.2)	·
8	·	143 (8.5)	·	168.0 (27)		·	193.6 (8.7)		·	8			·	88.4 (39)						·	119.2 (1.5)	·
9	·	118 (2.1)	·	141.2 (21)		·	189.3 (8.8)		·	9			·	86.2 (28)	[·	62.2 (1.8)]				·	117.4 (1.4)	·
10			·	142.2 (44)		·	192.7 (9.7)		·	10			·	80.5 (50)	[·	68.9 (1.5)]				·	117.1 (1.6)	·
11			·	129.1 (59)		·	189.4 (10)		·	11	·	62 (4.3)	·	84.4 (32)	[·	75.9 (1.3)]				·	114.6 (1.8)	·
12			·	137.2 (51)		·	191.2 (9.6)		·	12			·	85.3 (61)	[·	81.5 (1.8)]				·	114.8 (2.1)	·
14			·	134.2 (56)		·	187.7 (10)		·	14			·	90.3 (63)	·	91[i] (2.8)[i]				·	113.6 (2.6)	·
16			·	130.6 (62)		·	180.6 (11)		·	16			·	94.0 (71)	[·	94 (2.4) [j]]	·	107.1 (*h*)		·	111.2 (3.7)	·
18			·	130.1 (71)		·	175.3 (11)		·	18			·	90.6 (73)	[·	90 (0.46) [j]]	·	110.4 (5.0)				·
Cu3-*n*										**L3**-*n*												
3			·	227.8[e] (46)					· [f]	3			·	119.5 (31)						·	145.0 (0.82)	·
4			·	222.7[e] (45)					· [f]	4			·	116.3 (38)						·	147.2 (1.1)	·
5			·	225.6[e] (51)					·	5			·	97.9 (25)						·	136.9 (0.69)	·
6			·	222.7[e] (52)					·	6			·	98.1 (30)						·	139.6 (0.92)	·
7			·	218.4[e] (54)					·	7			·	88.0 (36)						·	134.3 (1.0)	·
8	·	80 (2.6)	·	208.9 (51)					·	8			·	97.5 (34)						·	133.6 (1.2)	·
9	·	*g*	·	200.7 (51)					·	9	·	78 (*c*)	·	82.5 (35)						·	132.1 (1.3)	·
10	·	101 (6.9)	·	198.3 (49)					·	10	·	78 (11)	·	86.6 (38)						·	130.9 (1.2)	·
11	·	97 (8.1)	·	198.0 (49)					·	11			·	85.4 (43)						·	129.6 (1.2)	·
12	·	114 (14)	·	195.8 (49)					·	12			·	90.3 (52)						·	128.2 (1.7)	·
14	·	112 (21)	·	191.1 (49)					·	14			·	94.2 (58)						·	125.5 (1.9)	·
16	·	113 (26)	·	188.6 (49)					·	16			·	96.7 (67)			·	114.2 (*h*)		·	122.3 (2.7)	·
18	·	115 (36)	·	184.4 (48)					·	18			·	99.5 (75)			·	118.6 (*h*)		·	120.1 (4.0)	·

[a] Minimum estimate with some decomposition suspected. [b] Inseparable from solidification. [c] Not measurable due to broadness. [d] Included in its preceding process. [e] Split peak. [f] Decomposition. [g] A two-hump endothermic event was observed over 67−81 °C (1.9−2.8 kJ mol^{-1}), which is reproducible and reversible. [h] Included in its following process. [i] Resolved on cooling. [j] An estimate from a broad peak.

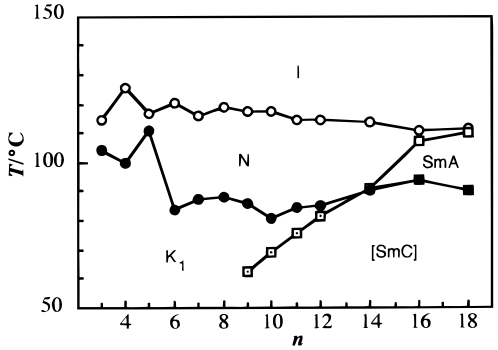

Figure 6. Phase pattern diagram for the homologous series **L2**.

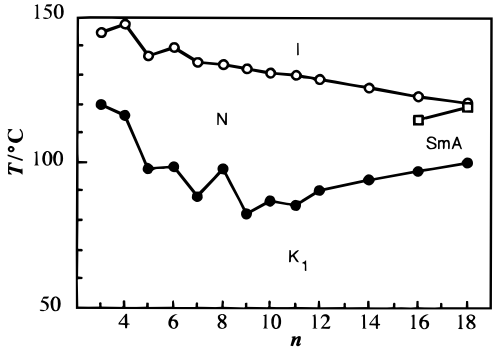

Figure 7. Phase pattern diagram for the homologous series **L3**.

thermal stability of the N phases is lower for series **L2** than for **L1**. These new features of mesomorphism in series **Cu2** and **L2** can be ascribed to the interactions involving polar carbonyl groups[9] incorporated in the *N*-phenyl moiety.

Turning to the third series, **Cu3**, in which the salicylidene moiety is attached by the alkanoyloxy group, the situation suddenly changes. This series is nonmesogenic while a systematic solid−solid transition line has been recognized (Figure 4). On the other hand, the phase pattern of the series **L3** is very close to that of series **L1** with only slight enhancement in both N and SmA phases (Figures 5 and 7). Some intermolecular interactions involving the metal center should be responsible for the rise in melting points. One of the factors is probably the weak axial coordination of the carbonyl oxygen to a neighboring copper center in the solid state. Degree of polarization and formation of a coordination bond may be probed by the C═O stretching vibrational frequency. Figure 8 shows the infrared absorption spectra of **Cu2**-10 and **Cu3**-10, recorded at elevated temperatures. Relevant carbonyl absorptions occur at 1760 cm^{-1} (65 °C, K_1) for **Cu2**-10 and 1753 cm^{-1} (90 °C, K_2) for **Cu3**-10. In their liquid states, these peaks shift to 1764 and 1761 cm^{-1}, respectively. The shift to higher energy in **Cu3**-10 is twice that in **Cu2**-10. It should be noted that the reference peaks due to skeletal vibrations at 1606−1612 cm^{-1} show practically no shift over the same temperature range. Incidentally, the absorption observed in the SmA phase of **Cu2**-10 is at 1763 cm^{-1} (at 168 °C), which is closer to the value in its liquid state.

The above comparison supports the view that the carbonyl group in **Cu3**-*n* is involved in the coordinative interaction, to a greater extent in the crystalline phase. Presumably the effect is less significant when the carbonyl group is placed in a small, more mobile fragment of the molecule as in **Cu2**-*n*. To be more specific to the crystalline state, it is recalled that smectogenic

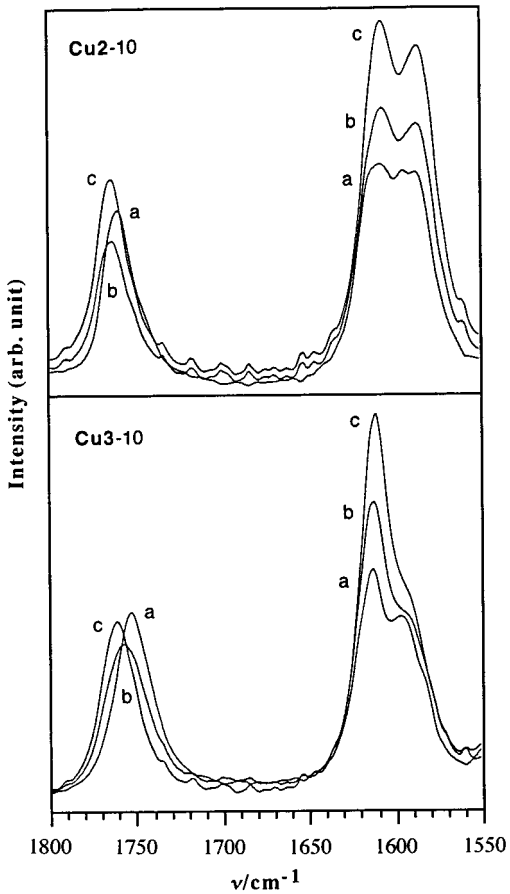

Figure 8. Infrared spectra of **Cu2**-10 (top) at (a) 65, (b) 168, and (c) 214 °C and of **Cu3**-10 (bottom) at (a) 90, (b) 150, and (c) 221 °C.

compounds tend to crystallize in layers,[10] where rodlike molecules are aligned parallel to each other (prosmectic). Translational freedom along the molecular long axis that runs more or less parallel to the RO---Cu---OR direction in the present lathlike molecules would be largely affected if the chemical link of group R is changed but not so much by a change in R′. We suppose that a potential smectic phase in **Cu3**-*n* would be at least comparable to those for the other two counterparts, but its observation is simply hampered by the crystalline phase that has been even more greatly stabilized. It can be further speculated that the smectic array of **Cu3**-*n* molecules might be tilted due to the dipolar interactions. Sirigu et al. have reported that several analogous complexes with R = R′= alkanoyl (heptanoyl to dodecanoyl) groups actually exhibit enantiotropic SmC phases.[6b] This literature example demonstrates that there is a way to disturb the crystal stability and uncover a mesophase in the copper complex carrying terminal alkanoyloxy substituents, although the higher molecular symmetry with four long chains of equal length may be responsible for the particular phase incidence in this case. Another example of smectic phases revealed in copper(II) salicylaldimines with terminal alkanoyloxy substituents was reported recently.[11] The bulky, chiral 2-chloro-3-methylbutyroyl group employed in this study may perturb the crystal packing in a convenient way.

Layer Structure of the Smectic Phases. The mesomorphic behaviors of our complexes **Cu1**-*n* and **Cu2**-*n* are thus quite

(9) Gray, G. W. In *Advances in Liquid Crystals*; Brown, G. H., Ed.; Academic Press: New York, 1976; Vol. 2, p 1.

(10) Kelker, H.; Hatz, R. *Handbook of Liquid Crystals*; Verlag Chemie: Weinheim, 1980; p 224.

(11) Tian, Y.-Q.; Su, F.-G.; Xing, P.-X.; Zhao, X.-Y., Tang, X.; Zhao, X.-G.; Zhou, E.-L. *Liq. Cryst.* **1996**, *20*, 139.

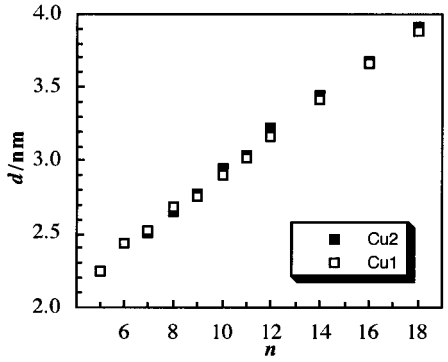

Figure 9. Plots of smectic layer distances for series **Cu1** and **Cu2**.

straightforward, each showing only the SmA phase which is common among as many as twenty-two homologues. It is particularly intriguing that in no case has an N phase been found above it. The propensity of SmA phases among liquid crystalline copper(II) complexes of two-ring *N*-salicylideneaniline derivatives has been pointed out,[2a] and the present work reinforces the trend.

We have carried out powder X-ray diffraction (XRD) measurements for all of the enantiotropic members of series **Cu1** and **Cu2**. The XRD profiles of these SmA phases are consistent with fluid lamellar structure. The second-order Bragg reflections were detected for most of the compounds, and they were more intense than the first-order peaks in cases of **Cu1**-*n* (n = 14, 16, 18). The values of smectic layer distance, d, are plotted in Figure 9 as a function of n. Determinations over a range of reduced temperatures of $T/T_{AI} = 0.96-0.99$, where T_{AI} is the SmA−I transition point, are plotted together because the temperature dependence of d was actually not very strong. The two data sets in Figure 9 can be fitted with practically identical linear equations, d(**Cu1**)/nm = 1.651 + 0.125n and d(**Cu2**)/nm = 1.642 + 0.128n. Thus the change in R′ between ethyl and acetyl groups has no effect on the static structure of these SmA phases, and a common structural model applies.

The linear relationship between d and n can be taken as evidence for the structural uniformity within the homologous series. The slope indicates that the smectic layer expands with increasing n by the amount for only one methylene unit. This condition is met by assuming full interdigitation of the all-trans alkyl chains of R along the layer normal, and the intercept value, 1.6 nm, is in good agreement with an estimate from a CPK model.

A comparison among the smectogenic ligands **L1**-*n*, **L2**-*n*, and **L3**-*n* (n = 16 and 18) is useful. The **L1** ligands yielded d = 4.33 nm (n = 16) and 4.58 nm (n = 18) at $T/T_{AI} = 0.97$. Since their molecular length, l, is estimated to be 3.61 and 3.89 nm, respectively, the molecules must slide out of a layer to some extent. This would lead to a model in which the very long alkyl chains are interdigitated and orthogonally packed. This model is reminiscent of that for the copper complexes, but the ligand cores are only arranged in head-to-head configuration and not chemically bonded. The layer spacings are similar with ligands **L3**-16 and **L3**-18 (4.12 and 4.50 nm), which seem to involve a good packing of alkanoyl chains. The small decrease (compared to **L1**-*n*) may be ascribed to a different chain orientation due to the carbonyl insertion. On the other hand, the terminally acetoxy-substituted ligands **L2**-16 and **L2**-18 exhibited much larger spacings (5.80 and 5.98 nm), and their SmA phases now seem to fit a dimer SmA model (d/l = 1.5−1.6). The nature of the core−core interaction is likely to be predominantly dipolar, and this is also reflected generally in the mesophase stability as discussed above. Although it could not be measured accurately, the monotropic SmA → SmC transitions in **L2**-*n* (n = 16 and 18) were weakly first order (Table 1), which is distinctive from usual monolayer smectics. In fact, the DSC endothermic peak for N → SmC transition in **L2**-14 is also broadened and the event may be better assigned to N → SmA → SmC transitions, though it is not identifiable optically. The SmC phases of **L2**-*n* (n = 11, 12, 14) also have very large lattice constants (5.35, 5.59, and 5.73 nm, respectively, at $T/T_{CA} = 0.92-0.97$) with up to third-order reflections observed, and they must also comprise dimerized molecular units.

Thus the effect of polar carbonyl groups is quite different between the organics and the metal species in both of thermal and structural aspects. One at the foot of R′ distinguishes the ligands, and the other at the foot of R strongly discriminates the complexes.

Thermodynamic Parameters. The above structural motif for the metallosmectic A phase has a precedent among a smaller group of compounds.[7c,12] Possibilities that the terminal alkyl chains are either interdigitated or crumpled have been previously argued.[12a] The two models are conceptually different if we evaluate the intermolecular forces acting in the SmA phases. There is no evidence favoring one model over the other for our complexes, and actually both of them may apply depending on the relative size of metal chelate to the alkyl tails. It helps for our purposes just to imagine the process of forming a smectic array. The bis[*N*-(4-Y-phenyl)salicylaldiminato]copper(II) cores alone would have a tendency to lie more or less parallel to each other.[13] When 4-alkoxy chains are incorporated and molecular rotation sets in, the terminal void must be filled with the alkyl groups, the ordering of which must be adjusted in each case of n for maximum adhesion. It should be noted that in no case does the system choose to tilt the molecules so as to minimize the void volume. This suggests that the orthogonal mode of packing is important for the van der Waals interaction between the alkyl chains.

The crystal structure of bis[4-*n*-dodecyloxy-*N*-(4-*n*-propylphenyl)salicylaldiminato]copper(II), which carries unbalanced tails and is very similar to our **Cu1**-12, has been reported.[14] The terminal dodecyl chains are ordered in the all-trans conformation and packed in the fully interdigitated configuration with equal distances (4.29−4.30 Å) among the chains. Molecular strata are tilted in this crystal, but once molten they must transform to an orthogonal array to form the SmA phase. According to the principle of projection−hollow packing,[2d] the explicitly layered disposition of molecules involves an intralayer interaction energy that is several times greater than the interlayer interaction energy. The interlayer chain−chain interaction is regarded as weak and rather lubricating between the layers. We were interested to see how far such a simplified (and convenient) view is valid, and we analyzed thermodynamic parameters for

(12) (a) Ghedini, M.; Armentano, S.; Bartolino, R.; Torquati, G.; Rustichelli, F. *Solid State Commun.* **1987**, *64*, 1191. (b) Levelut, A. M.; Ghedini, M.; Bartolino, R.; Nicoletta, F. P.; Rustichelli, F. *J. Phys.* **1989**, *50*, 113.

(13) Ghedini and co-workers have reported[12b] on some intralayer nematic-like correlation of about 0.85 nm in the SmA phases of copper(II) complexes related to **Cu1**-7 and **Cu1**-12 (butyl groups are attached in place of the ethoxy groups) and a side-by-side pair configuration has been suggested. We once observed two sets of reflections for **Cu2**-18, one of which contained a maximum at angles corresponding to 0.93−0.94 nm. This was not reproduced when experiments were repeated later.

(14) Armentano, S.; De Munno, G.; Ghedini, M.; Morrone, S. *Inorg. Chim. Acta* **1993**, *210*, 125.

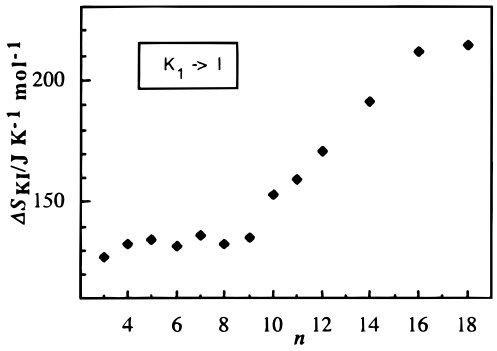

Figure 10. Plot of the entropy changes ΔS_{KI} associated with $K_1 \rightarrow I$ transitions in **Cu1**-*n*.

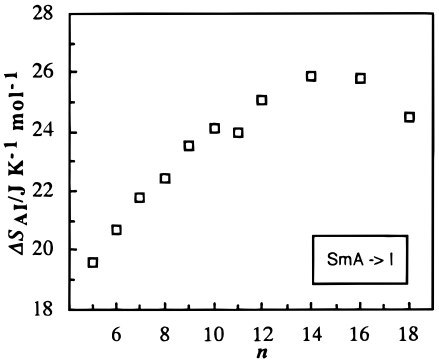

Figure 11. Plot of the entropy changes ΔS_{AI} associated with SmA−I transitions in **Cu1**-*n*.

the chain ordering as described below. Incidentally, the role of attached alkyl groups in forming a smectic structure would be different if the core alignment is dominated by other strong interactions such as dipole−dipole and/or polar group-to-metal interactions. We have investigated new series in which the groups R′ in **Cu2**-*n* were extended, and preliminary results have been reported elsewhere.[15]

It is hoped here that the relative contributions from the rigid core part of the molecule and the flexible alkyl tails to the order in the above metallosmectic A phase could be drawn from the dependence of thermodynamic parameters on the length of terminal alkyl chains. According to the phenomenological theories for melting of molecular crystals,[16] the entropy of fusion, S_f, can be expressed as

$$S_f = \Delta S_{pos} + \Delta S_{or} + \Delta S_{con} + \text{etc.} \quad (1)$$

Here the specified terms represent changes upon fusion in positional, orientational, and "configurational" entropies, respectively. The term ΔS_{con} takes into consideration the configurational freedom of the flexible alkyl chain, and it may be split into two terms as in

$$\Delta S_{con} = S_0 + nS \quad (2)$$

Equation 1 can then be rewritten as a function of *n*,

$$S_f = (\Delta S_{pos} + \Delta S_{or} + S_0) + nS = S_{f0} + nS \quad (3)$$

The "fusion" takes place in stages in liquid crystalline materials, and we can still analyze the total entropy change between crystalline and isotropic liquid states and then partition a part of the acquired entropy of the liquid to the mesophase. The complexes **Cu1**-*n* are suited to this study, since the entire series of enantiotropic mesophases ($n = 5-18$) can be described by a common structural model, and the thermal stability does not vary too much from one homologue to another. Of additional importance is the fact that the crystalline polymorphism is relatively less complicated, and the values confirmed for the K_1 phase can be used for the analysis. A plot in Figure 10 shows the dependence on *n* of the entropy changes, ΔS_{KI}, associated with $K_1 \rightarrow I$ transitions in **Cu1**-*n*. It is seen that the value of ΔS_{KI} alternates around 130−135 J K^{-1} mol^{-1} for $n \leq 9$ but then starts to increase nearly linearly with *n*. Least-squares fitting to the linear portion ($9 \leq n \leq 16$) of the curve leads to an estimate of the terms in eq 3 as $S = 10$ J K^{-1} mol^{-1} and $S_{f0} = 45$ J K^{-1} mol^{-1}. A theoretical prediction for the linear term *S* is 9.13 J K^{-1} mol^{-1} ($nS = R \ln 3^n$) and values found for triclinic (even *n*) and hexagonal (odd *n*) *n*-alkanes are 10.8 and 7.66 J K^{-1} mol^{-1}, respectively.[17] The present estimate of *S* is on the same order and close to the triclinic case. However, the *virtual* intercept S_{f0} is several times greater compared to the S_{f0} of *n*-alkanes (10.0 J K^{-1} mol^{-1} for even *n*).[17] The value of ΔS_{KI} actually levels at 134 J K^{-1} mol^{-1} (averaged over $4 \leq n \leq 9$). The complexes are better regarded as a paraffin molecule "loaded" with a core part in the middle.[16] It appears that the load is so heavy that the core interaction overwhelms any series effect for the lower members **Cu1**-*n* ($n = 3-9$).

The total entropy change ΔS_{KI} consists of changes upon $K_1 \rightarrow$ SmA (ΔS_{KA}) and SmA−I (ΔS_{AI}) transitions for the mesomorphic members **Cu1**-*n* ($n = 5-18$). It is dominated by the former, and ΔS_{KA} naturally shows a dependence on *n* similar to that of ΔS_{KI}. Linear fitting for the region $9 \leq n \leq 16$ yields an intercept and a slope of 24 and 10 J K^{-1} mol^{-1}, respectively. This indicates that the paraffin characters of the higher homologues of **Cu1**-*n* show up in their melting transitions. Heavy loading of the core is recognized again, which amounts to an entropy change of 113 J K^{-1} mol^{-1} on the average. On the other hand, a plot of ΔS_{AI} vs *n* in Figure 11 shows that the amount of entropy gain upon clearing is no longer very dependent on *n*. Instead, the plot contains a portion linear to *n* among lower homologues. The slope of 0.97 J K^{-1} mol^{-1} for the region of $5 \leq n \leq 9$ suggests that the short chains in these compounds are still somewhat ordered configurationally until the phase clears. The intercept of 15 J K^{-1} mol^{-1} is only a little greater than S_{f0} of *n*-alkanes.

It is not certain how to signify the borderline value of $n = 9$. The lowest member of **Cu1** exhibiting an enantiotropic SmA phase is **Cu1**-5, and its molecular length is estimated to be 2.9 nm; this is near the limit of the length/breadth ratio based upon hard rod models for the orientational ordering, assuming a molecular breadth of ca. 0.9 nm. The actual "lattice constant" for the SmA phases present is shorter than the model length, and 2.8 nm is realized with **Cu1**-9. This happens to be the starting point of the linear series effect seen above.

Similar analysis of ΔS vs *n* was attempted for series **Cu2**. The main conclusion as to the linear dependence toward large *n* is the same, but the core loading was not clearly recognized because the entropy data were more scattered. However, an estimate from the melting process was no greater than about 80 J K^{-1} mol^{-1} and definitely smaller than that for the series **Cu1**. The SmA−I entropy is also generally smaller for **Cu2**-*n* in comparison to **Cu1**-*n*. Series **Cu3** shows a nearly constant

(15) Hoshino-Miyajima, N.; Sekiuchi, T.; Yamazaki, W.; Sasaki, T.; Matsunaga, Y. *Mol. Cryst. Liq. Cryst.* **1996**, *286*, 311.
(16) Ubbelohde, A. R. *The Molten State of Matter*; Wiley: Chichester, U.K., 1978.
(17) Broadhurst, M. G. *J. Res. Natl. Bur. Stand., Sect. A* **1962**, *66A*, 241.

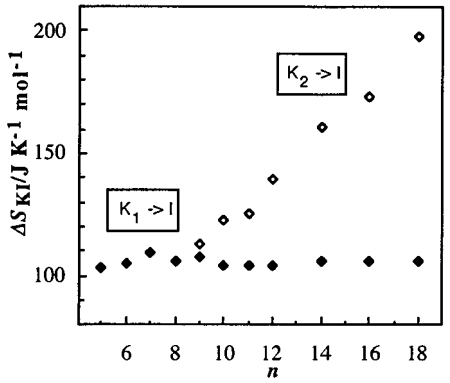

Figure 12. Plot of the entropy changes ΔS_{KI} associated with $K_2 \rightarrow I$ and $K_1 \rightarrow I$ transitions, respectively, in **Cu3**-*n*.

entropy of melting at 106 J K^{-1} mol^{-1} for the K_1 crystals throughout the series, but a deflection appears again at $n = 9$ if ΔS_{KK} values for the $K_2 \rightarrow K_1$ processes are added (Figure 12). An analogy holds in this respect between the K_1 phase of series **Cu1** and the K_2 phase of series **Cu3**. On the other hand, the basic features of melting processes of the three ligand series are similar to each other; the entropy change increases gradually with *n*. Small entropy changes associated with N−I transitions for most of the ligand homologues were not amenable to a quantitative analysis, but they also seem to be a rather smooth function of the chain length.

Concluding Remarks. Arbitrary choice of alkyl groups for metallomesogens may not always work as intended. It can be misleading sometimes; our complexes **Cu1**-5 and **Cu1**-12, for example, have practically the same clearing points, and by working only in cooling runs, as is often the case, one might easily overlook the major difference in the chain dynamics. Relatively long alkyl chains have been (and often must be) employed in metallomesogens, and this tends to result in high-viscosity liquid crystals. Metal complexes are unique cores, and suitable alkylation schemes would have to be worked out in each case when designing specific new materials.

Experimental Procedures

Materials. Synthetic pathways for the ligands are outlined below. Specific procedures were adapted from the literature methods.

L1-*n*. A 4-alkoxy-2-hydroxybenzaldehyde was obtained by alkylating 2,4-dihydroxybenzaldehyde.[3] Higher homologues ($n = 11-18$) were isolated and purified by recrystallizing from methanol, while the other members were used as extracted with benzene from the reaction mixture. Schiff base condensation with *p*-phenetidine was carried out in refluxing ethanol, and the product was recrystallized repeatedly from either an ethanol/benzene mixture or ethanol alone until constant phase transitions were observed. Yields: 50−60%. ^{1}H NMR (400 MHz, $CDCl_3$) for **L1**-9: δ 13.89 (s, 1H, OH), 8.49 (s, 1H, azomethine), 7.24 (d, $J = 8.5$ Hz, 1H, salicyl 6′-), 7.22 (d, $J = 8.6$ Hz, 2H, aniline 2,6-), 6.92 (d, 2H, 3,5-), 6.50 (d, $J = 2.4$ Hz, 1H, 3′-), 6.47 (dd, 1H, 5′-), 4.05 (q, $J = 6.7$ Hz, 2H, ethyl CH_2), 3.99 (t, $J = 6.7$ Hz, 2H, nonyl 9-CH_2), 1.79 (quintet, 2H, 8-CH_2), 1.43 (t, 3H, ethyl CH_3), 1.43−1.28 (m, 12H, methylenes), 0.89 (t, 3H, 1-CH_3). ^{13}C NMR (101 MHz, $CDCl_3$) for **L1**-9: δ 163.8, 163.3 (phenyl 4, salicyl 4′), 159.5 (azomethine), 157.8 (2′), 141.1 (1), 133.2 (3′), 122.0, 115.2 (2,6, 3,5) 113.0 (1′), 107.5, 101.6 (5′, 6′), 68.2 (nonyl 9-CH_2), 63.8 (ethyl CH_2), 31.9, 29.5, 29.4, 29.3, 29.1, 26.0, 22.7 (methylenes), 14.8, 14.1 (CH_3).

L2-*n*. The benzaldehyde derivative prepared as above was condensed with *p*-aminophenol either in boiling toluene (for $n = 11-18$) or in ethanol at ambient temperature. Esterification by the DCC method[18] with acetic anhydride led to the desired product, which was purified by column chromatography eluting with chloroform. Yields: 20−30%. ^{1}H NMR (400 MHz, $CDCl_3$) for **L2**-9: δ 13.56 (s, 1H, OH), 8.50 (s, 1H, azomethine), 7.26 (d, $J = 8.5$ Hz, 1H, salicyl 6′-; 2H, phenyl 3,5-), 7.13 (d, 2H, 2,6-), 6.51 (d, $J = 2.4$ Hz, 1H, 3′-), 6.49 (dd, 1H, 5′-), 4.00 (t, $J = 6.7$ Hz, 2H, nonyl 9-CH_2), 2.31 (s, 3H, acetyl CH_3), 1.80 (quintet, 2H, 8-CH_2), 1.46 (quintet, 2H, 7-CH_2), 1.28 (m, 10H, methylenes), 0.89 (t, 3H, 1-CH_3). ^{13}C NMR (101 MHz, $CDCl_3$) for **L2**-9: δ 169.5 (C═O), 163.8, 161.7 (phenyl 4, salicyl 4′, azomethine), 149.0 (2′), 146.2 (1), 133.6 (3′), 122.5, 121.9 (2,6, 3,5) 112.8 (1′), 107.8, 101.6 (5′, 6′), 68.3 (nonyl 9-CH_2), 31.9, 29.5, 29.4, 29.3, 29.1, 26.0, 22.7, 21.1 (acetyl CH_3, methylenes), 14.1 (1-CH_3).

L3-*n*. 4-Ethoxy-*N*-(2,4-dihydroxybenzylidene)aniline[3] was subjected to the DCC esterification[18] with *n*-alkanoic acid. Purification was effected by repeated recrystallization from methanol/benzene mixtures. Yields: 50−70%. ^{1}H NMR (400 MHz, $CDCl_3$) for **L3**-9: δ 13.76 (s, 1H, OH), 8.58 (s, 1H, azomethine), 7.35 (d, $J = 8.8$ Hz, 1H, hydroxyphenyl 5-), 7.25 (d, $J = 8.8$ Hz, 2H, phenyl 2′,6′-), 6.93 (d, 2H, 3′,5′-), 6.74 (d, $J = 2.4$ Hz, 1H, 2-), 6.67 (dd, 1H, 6-), 4.05 (q, $J = 7.0$ Hz, 2H, ethyl CH_2), 2.55 (t, $J = 7.6$ Hz, 2H, nonanoate 8-CH_2), 1.75 (quintet, 2H, 7-CH_2), 1.43 (t, 3H, ethyl CH_3), 1.31 (m, 10H, methylenes), 0.89 (t, 3H, 1-CH_3). ^{13}C NMR (101 MHz, $CDCl_3$) for **L3**-9: δ 171.8 (C═O), 162.4 (hydroxyphenyl 1), 159.4 (azomethine), 158.3 (phenyl 4′), 154.1 (3), 140.9 (1′), 132.7 (2), 122.3, 115.2 (3′,5′, 2′,6′), 117.3 (4), 112.7, 110.3 (6, 5), 63.8 (ethyl CH_2), 34.5, 31.8, 29.2, 29.1, 24.9, 22.6 (methylenes), 14.8, 14.1 (CH_3).

Copper complexes were prepared and purified in a way similar to the previous methods.[3] Anal. Calcd for **Cu1**-5, $C_{40}H_{48}N_2O_6Cu$: C, 67.06; H, 6.75; N, 3.91. Found: C, 67.05; H, 6.86; N, 4.08. Calcd for **Cu2**-7, $C_{44}H_{52}N_2O_8Cu$: C, 66.02; H, 6.55; N, 3.50. Found: C, 66.11; H, 6.59; N, 3.47. Calcd for **Cu3**-9, $C_{48}H_{60}N_2O_8Cu$: C, 67.31; H, 7.06; N, 3.27. Found: C, 67.27; H, 7.01; N, 3.40.

Physical Measurements. Differential scanning calorimetry was performed on Rigaku Thermoflex and TAS100 calorimeters with typical scanning rates of ± 5 K min^{-1}. Thermal annealing in the solid state of a pristine sample was applied when necessary. Fresh solid was employed each time, and data from the first heating runs were used (heat for N−I transitions include pretransitional effects). Heat measurements involved variance of 8% at most, and only rounded averages are listed in Table 1. The entropy values were calculated directly from the DSC data, but the data points plotted in Figures 10−12 also represent mean values. X-ray diffraction measurements were carried out using a Rigaku RAD IVB and a MacScience MXP3 autodiffractometers with Ni-filtered Cu Kα radiation. A home-built sample holder was used, and the low-angle data were calibrated with stearic acid in a monoclinic form ($d_{001} = 3.987$ nm). Infrared spectra were recorded with a Perkin-Elmer 1600 series FT-IR instrument, fitted with an OMRON model E5T temperature controller.

Solid-state polymorphism in series **Cu1** was worked out to distinguish three major polymorphs. Isolated solids were subjected to routine XRD measurements at room temperature, and the largest periodicities of the molecular long axis dimension, d_1, were classified. It was possible to fit the data points to two straight lines, d_1(D)/nm = 1.383 + 0.114*n* and d_1(L)/nm = 1.318 + 0.108*n* as empirical guides, with the exception of **Cu1**-18. Crudely speaking, this grouping happened to correspond to the physical appearances of dark brown (D), granular-to-flaky crystals and to light brown (L) flaky crystals. However, the story was not so simple; the XRD data for **Cu1**-10 which appeared to be in group D revealed that it contained the group L species as well, and different batches of recrystallization for **Cu1**-16 in group L yielded a group D solid and another form (perhaps solvated), and so on. In these cases, DSC experiments with annealed samples showed that the group D samples can be easily converted to the crystalline form K_1 having a higher melting point (by 2 °C) while the group L solids were unchanged. On the other hand, **Cu1**-18 formed a crystal with a greenish tint, the d_1 value for which fell between the above two lines. It showed a color change to group L appearance and a decrease in d_1 upon heating, but it varied depending on the conditions. Therefore the calorimetric data in K_1 listing of **Cu1**-18 in Table 1 may be underestimated, otherwise this complex would not conform to the series behavior.

Cu3-*n* complexes recrystallized commonly from ethanol/benzene mixtures showed little heat anomalies, and the data obtained with these

(18) Hassner, A.; Alexanian, V. *Tetrahedron Lett.* **1978**, 4475.

light brown flaky crystals are compiled in Table 1. Crystals of **Cu2**-*n* complexes were brown and had a more fibrous appearance, except for **Cu2**-4 which was green. These acetoxy-substituted complexes (and some lower alkanoyloxy homologues of **Cu3**) were more prone to hydrolysis and repeated recrystallizations and/or usual storage under air led to some degradation as evidenced by decreases in the phase transition temperatures of 3−10 °C. Besides, isolated solids of higher members of the series **Cu2**-*n* ($n \geq 8$) were richer in polymorphism, which was not easily sorted out over manageable durations of annealing. Single-phase specimens were obtained by partial melting for these derivatives. Therefore, while the temperature data listed in Table 1 for **Cu2**-*n* are the highest observed for freshly purified samples, the enthalpy data are those collected with pristine, unrecrystallized ($n = 3$ and 4), solid-state annealed ($n = 5-7$), or melt−crystallized samples ($n \geq 8$, and run exceptionally at 10 K min^{-1}).

Solid states of the ligands were not deeply investigated either, and only routine annealing was applied. Therefore, some of the data may contain latent heat of unspecified transitions such as desolvation.

Acknowledgment. This work was supported by the Grants-in-Aid for Scientific Research, Nos. 04804048 and 06453045, from the Ministry of Education, Science, Sports and Culture of Japan and partly by a fund from Hayashi Memorial Foundation for Female Natural Scientists.

IC9710566